Motional decoherence in ultracold-Rydberg-atom quantum simulators of spin models

Zewen Zhang [1,2,*] Ming Yuan [1,2,3,†] Bhuvanesh Sundar [1,2,4,‡] and Kaden R. A. Hazzard [1,2]

[1] *Department of Physics and Astronomy, Rice University, Houston, Texas 77005, USA*
[2] *Rice Center for Quantum Materials, Rice University, Houston, Texas 77005, USA*
[3] *School of the Gifted Young, University of Science and Technology of China, Hefei 230026, China*
[4] *JILA, Department of Physics, University of Colorado, Boulder, Colorado 80309, USA*

(Received 30 May 2024; revised 14 October 2024; accepted 13 November 2024; published 27 November 2024)

Ultracold Rydberg-atom arrays are an emerging platform for quantum simulation and computing. However, decoherence in these systems remains incompletely understood. Recent experiments [Guardado-Sanchez *et al.*, Phys. Rev. X **8**, 021069 (2018)] observed strong decoherence in the quench and longitudinal-field-sweep dynamics of two-dimensional Ising models realized with ^{6}Li Rydberg atoms in optical lattices. This decoherence was conjectured to arise from the effective spin $\frac{1}{2}$ formed by the ground and Rydberg electronic states coupling to atom motion and therefore inducing an effective interaction noise. Here we show that this spin-motion coupling indeed leads to decoherence in qualitative, and often quantitative, agreement with the experimental data, by treating the difficult spin-motion-coupled problem using the discrete truncated Wigner approximation method. We also show that this decoherence will be an important factor to account for in future experiments with Rydberg atoms in optical lattices and microtrap arrays and discuss methods to mitigate the effect of motion, such as using heavier atoms or deeper traps.

DOI: 10.1103/PhysRevA.110.053321

I. INTRODUCTION

Arrays of Rydberg atoms, built via either optical lattices [1–3] or programmable microtraps [4–14], provide a versatile platform for studying quantum many-body systems, including their real-time dynamics. Recent experiments have realized synthetic quantum magnetic systems by constructing Rydberg-atom lattices with blockade radii R_b that are comparable to the lattice constants a_l [7–17]. Such systems are widely used in areas like controlling many-body quantum phases [12–16] and studying out-of-equilibrium dynamics [7–9,17].

While many of these experiments are conducted on timescales where the atom motion is negligible [9], recent experiments [18] have revealed significant discrepancies between the experimental results and the theoretical predictions even after accounting for single-particle decoherence. Although Ref. [18] qualitatively explained this discrepancy by introducing a two-body interaction noise, the explanation did not predict the magnitude of the noise or its dependence on system parameters, and this magnitude must be fit to the experimental data. Reference [18] suggests the noise is likely to be an effect of atom motion, which becomes important on the timescale $Jt \sim 1$, where J is the strength of interaction between atoms. Although some theories of atom motion in Rydberg-atom systems have been developed, these have focused on few-atom motional effects or low-lying motional excitations [19–27]. Now, understanding motional effects in a many-body setting is crucial for an emerging generation of experiments [7,8,28–32].

In this paper we show that the experimentally observed deviations from the expected Ising model are consistent with the effects of atom motion, which strongly supports atom motion as a source of the interaction noise observed in Ref. [18], and our calculations allow us to predict its effects in a wide range of experiments. There are two contributions from the atom motion: The first comes from the initial state's quantum and thermal spread of positions and momenta and the second comes from the interaction-induced motion during the dynamics.

To capture the role of atom motion without introducing additional fitting parameters for the interaction noise, in this work we apply the discrete truncated Wigner approximation (DTWA) [33], a semiclassical stochastic phase-space method, which enables numerical simulation of the system, whereas exact methods are not possible due to the large motional Hilbert space that prevents solution by exact methods. We start from a microscopic quantum description of the Hamiltonian and single-particle decoherence processes, only using experimental inputs that have been measured and are independent of any interaction noise, e.g., the atom mass, van der Waals (vdW) coefficient C_6, and (in some calculations) the T_1 and T_2 rates of individual atoms. As an aside, we note that Refs. [34–36] have applied DTWA to quenches, while our results include both quench and ramp dynamics.

The prediction of motional decoherence in Rydberg-atom arrays is especially important for the future of the Rydberg-atom-array quantum simulation platform. We show that while

*Contact author: zewen.zhang@rice.edu
†Present address: Pritzker School of Molecular Engineering, The University of Chicago, Chicago, Illinois 60637, USA.
‡Present address: Rigetti Computing, Fremont, California, USA.

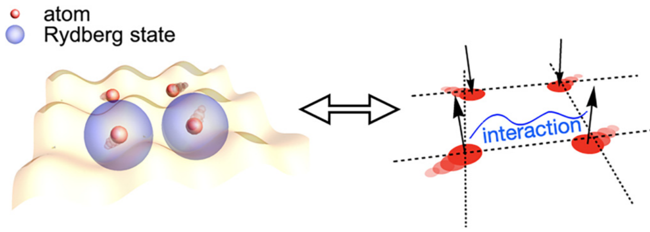

FIG. 1. A 2D optical lattice of atoms with two internal states coupled by a laser realizes a transverse-field Ising model with $|\downarrow\rangle$ and $|\uparrow\rangle$ given by the ground state $|g\rangle$ and the Rydberg state $|r\rangle$, respectively. Two atoms interact only if both are in $|\uparrow\rangle$, as described by Eq. (1). Spins (atoms) are allowed to move, as indicated by the pale red trails.

working with optical tweezers instead of a lattice reduces the motional decoherence, the decoherence nevertheless can be significant on timescales currently being experimentally explored [2,7,11]. Also, our calculations quantify how the decoherence depends on the depth of the tweezers or optical lattice, the atomic mass, and the sign of the interactions, providing a road map to mitigating the decoherence.

Our paper is structured as follows. Section II introduces the spin-motion-coupled Rydberg-atom lattice model and the DTWA method. Section III shows the dynamics following sudden quenches and slow detuning ramps, comparing the DTWA with and without motion. Section IV quantifies how the decoherence depends on experimental settings in optical lattices and microtraps. Section V summarizes and discusses considerations for future work.

II. MODEL AND METHOD

This section presents the spin-motion-coupled Ising model used to describe experiments of Rydberg atoms in optical lattices or microtrap arrays (Sec. II A) and the DTWA methods used to calculate the dynamics (Sec. II B).

A. Spin-motion-coupled Ising model

The experimental system we consider is an array of atoms in a two-dimensional (2D) square lattice at unit filling driven by a laser that couples ground-state atoms $|g\rangle = |\downarrow\rangle$ to a low-lying Rydberg state $|r\rangle = |\uparrow\rangle$, with Rabi frequency Ω and detuning Δ, as shown in Fig. 1. In the spin language, the Ω and Δ give transverse and longitudinal fields, respectively. There is an attractive van der Waals interaction when two atoms are in the Rydberg state, giving rise to an Ising coupling between spins that is C_6/R^6, where R is the distance between spins. The nearest-neighbor terms dominate for the parameters in Ref. [18], so we neglect longer-range interactions.

Atoms move due to their initial velocities and the vdW interaction among those in the Rydberg state and the trapping potential. Therefore, the Ising model must be extended to capture the kinetic energy and the optical forces on the atoms. We assume atom i is trapped by a 3D harmonic potential centered at lattice site i, which is valid in a deep lattice as long as the atoms are not too far displaced from their equilibrium position $\vec{R}_i$. Then the appropriate Hamiltonian is

$$H = \frac{\hbar}{2}\sum_i \left(\Omega\sigma_i^x - \Delta\sigma_i^z\right) - \frac{\hbar J}{4}\sum_{\langle i,j\rangle}\left(\frac{a_l}{r_{ij}}\right)^6 \left(\sigma_i^z+1\right)\left(\sigma_j^z+1\right) + \sum_{i,\alpha}\frac{p_i^{\alpha\,2}}{2m} + \sum_i \hbar V_0 \frac{\pi^2}{2a_l^2}\tilde{r}_i^{\,2}\left(1-\sigma_i^z\right), \tag{1}$$

where a_l is the lattice constant, $J = |C_6|/a_l^6$ is the nearest-neighbor interaction strength, p_i^α is the momentum of atom i in direction α ($\alpha = x, y, z$), σ_i^α is the Pauli matrix for atom i, r_{ij} is the distance between two atoms i and j that are located at $\vec{r}_i$ and $\vec{r}_j$, and $\tilde{r}_i$ is the magnitude of the displacement $\vec{\tilde{r}}_i = \vec{r}_i - \vec{R}_i$ of atom i from the center of the lattice site. As indicated by the last term, ground-state atoms are harmonically trapped and Rydberg-state atoms experience no trapping potential, as the antitrapping force on Rydberg-state atoms is usually smaller than the trapping force on ground-state atoms, as well as negligible compared to the Rydberg-Rydberg interaction. In the calculation, although the trapping force is kept on during the dynamics, it changes little of the dynamics, and the effects of the antitrapping force on Rydberg-state atoms would be even smaller, as shown in Appendix D.

Most of our concrete calculations are for ^{6}Li atoms in an optical lattice in the experimental configuration of Ref. [18], but the broad results apply more generally, for example, to other atoms and microtrap potentials, which are discussed in Sec. IV. When considering the experiments in Ref. [18], we take the lattice depth to be $V_0 = 55E_R/\hbar$, where $E_R = \pi^2\hbar^2/2ma_l^2$ is the recoil energy with $a_l = 1024/\sqrt{2}$ nm, and $C_6/a_l^6 = -2\pi \times 6.0$ MHz, the result from experimental fitting in Ref. [18]. Throughout our calculations, we neglect the single-particle decoherence unless otherwise specified. To measure how the system deviates from product states, we focus on the connected spin-spin correlation

$$C(i,j) = \langle\sigma_i^z\sigma_j^z\rangle - \langle\sigma_i^z\rangle\langle\sigma_j^z\rangle. \tag{2}$$

B. Discrete truncated Wigner approximation

In the area of quantum spin dynamics, the truncated Wigner approximation (TWA) methods are widely used, especially for quenches and when timescales are not too long. These methods are controlled approximations when the correlations between particles are small or the system is semiclassical [37]. Additionally, the DTWA method [33,38–40], which maps the spin degree of freedom to a discrete phase space, can also preserve oscillating features [35,36] and capture correlations [34] on moderate timescales; often, it outperforms the continuous TWA in 1D spin chains [40]. Recent studies [35,41–43] compare results from DTWA to exact results, higher-order DTWA calculations, or Rydberg-atom experiments and reveal that DTWA methods in 2D spin systems can be accurate for timescales of $Jt \simeq 2$. Truncated Wigner approximation methods approximate quantum dynamics by classical equations of motion (EOMs) propagated from the exact initial state's Wigner distribution (quasiprobability) [37]. The EOMs are derived from the Hamiltonian (1) and shown in Appendix A. We use the same random seed for calculations with different physical parameters.

For atoms in a harmonic trap with frequency ω at temperature T, the Wigner distribution is

$$W(x,p) = 2\tanh\left(\frac{\hbar\omega}{2k_BT}\right)\exp\left(-\frac{(x/\ell)^2+(p\ell/\hbar)^2}{\coth\left(\frac{\hbar\omega}{2k_BT}\right)}\right), \quad (3)$$

where $\ell = \sqrt{\hbar/m\omega}$ is the harmonic-oscillator length. In addition, $T = 0$ yields the ground-state Wigner distribution. For the spins, the DTWA represents the spin-$\frac{1}{2}$ observables as points in a discrete phase space [33,44], which we take to be the eight points $\vec{S}_u \in \frac{1}{2}(\pm1, \pm1, \pm1)$. Reference [40] showed that this choice of basis performs better than other choices in a broad range of scenarios [38]. When the initial spins are aligned in the $|\downarrow\rangle$ state, the quasiprobability $W(\vec{S}_u)$ is $\frac{1}{4}$ for the four points $\frac{1}{2}(\pm1, \pm1, -1)$ and 0 for the other four.

Our DTWA and exact diagonalization (ED) calculations are for a 4×4 lattice with periodic boundary condition. We have calculated results for a 6×6 system with the DTWA and they agree well with the 4×4 results. For example, for the long-time quench results discussed in Sec. III A 2, the differences of the correlation between two system sizes are always less (usually much less) than 6% for the range of Δ plotted, and for shorter times these differences are smaller. For both ED dynamics and solving the classical EOM, we use fourth-order Runge–Kutta with a time step of 1 ns for the ideal Ising model and 0.5 ns for the motional model. The results are well converged. For example, decreasing the integration time step by a factor of 2 for the ideal Ising long-time quench discussed in Sec. III A 2 changes all results by less than 2%. Therefore, in view of the comparison to ED methods and larger system sizes, the DTWA method we apply here is reliable to simulate the spin dynamics combined with motional degrees of freedom. Statistical errors are small, as indicated in the figures.

III. RESULTS: QUENCH AND RAMP DYNAMICS

A. Sudden quench

Motivated by Ref. [18], the first scenario we study is the quench dynamics of the Rydberg atoms in an optical lattice. Specifically, the lattice is initially filled with exactly one atom per site, which is in its electronic ground state (spin down) and in its motional ground state. (Section IV considers finite-temperature motional states as well.) After an instantaneous turn-on of Ω, the system evolves under Eq. (1). We study two quenches: short-time quenches with $\Omega t < \pi$ (Sec. III A 1) and long-time quenches with $\Omega t > \pi$ (Sec. III A 2). For each quench, we calculate the spin correlations $C(i, j)$ as a function of detuning Δ. To focus on the role of motional decoherence, other sources of decoherence are ignored in the quench dynamics.

1. Short-time quench

Figures 2(a) and 2(b) show that the effect of motion is small but observable for the short-time quench ($\Omega t = 0.5\pi$) dynamics. In these calculations, we use the Rabi frequency ($\Omega = 2\pi \times 4.1$ MHz) and duration ($t = 61$ ns) from the experiments in Ref. [18]. We compare three versions of the spin model: (i) the ideal Ising model with all spins sitting at the center of individual lattice sites; (ii) the frozen model, where each atom initially has a finite-width distribution of locations, given by Eq. (3), but does not move during the spin dynamics; and (iii) the full-motion model, where each atom has both an initial distribution of locations and momenta and it is allowed to move according to interactions with other atoms and the optical potential.

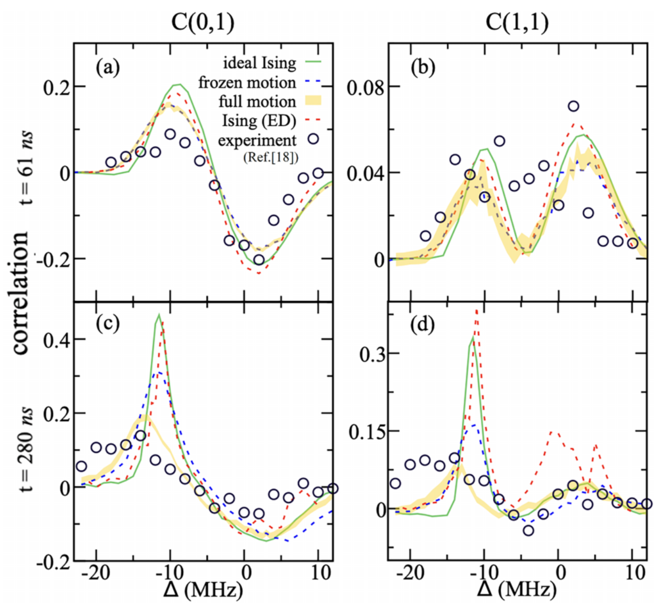

FIG. 2. Spin correlations at short duration [(a) and (b) $\Omega t = 0.5\pi$, 61 ns, 5000 DTWA trajectories] and at long duration [(c) and (d) $\Omega t = 2.97\pi$, 276 ns, 2000 DTWA trajectories] after a sudden quench with different Δ values. The circles represent experimental data from Fig. 2 in Ref. [18] and the curves show theoretical calculations described in the text. The shaded region indicates ±1 standard error of the mean and to avoid clutter are shown only on the full-motion results, which are the results with the largest statistical errors. In (b), while there is some apparent disagreement between simulation and experiment, one should note the very small scale of the vertical axis and thus the small absolute error.

Figures 2(a) and 2(b) show that the motion modifies the correlations even on these short timescales, as seen by comparing the ideal Ising and the full-motion model. However, for this timescale, the dominant contribution comes from the initial spread of atom positions rather than atom motion during the quench, evidenced by the close agreement between the full-motion and frozen-motion results.

Figure 2 also shows results obtained by 4×4 ED of the pure spin system. A comparison of this and the DTWA method confirms that the latter is an accurate approximation in the situations shown.

2. Long-time quench

Figures 2(c) and 2(d) show that atom motion significantly suppresses the growth of correlations in the long-time quench dynamics with $\Omega t = 2.97\pi$, using the corresponding experimental $\Omega = 2\pi \times 5.4$ MHz and $t = 276$ ns.

The simulations with atom motion qualitatively reproduce the experimental long-time quench results. Upon incorporating the initial-state effects and motion during the dynamics (the full-motion model), the height of the correlation peaks is dramatically reduced, in agreement with the experimental values. The atom motion also broadens and shifts the peaks. We also find that the frozen-motion model deviates strongly from the full-motion results. While some wiggles shown in the ED results do not appear in the DTWA results, our conclusion about the motional effects stands when comparing the motional results to coherent results.

A comparison of the short- and long-duration quenches demonstrates that the effects of motion increase over time. The evolution of correlations in both ideal Ising and full-motion models, as shown in Appendix B, confirms that the effect of motion accumulates over time and shows up after $t = 50$ ns in this experimental setting, independently of the detuning. A drastic increase of kinetic energy, specifically in the transverse direction, is also observed in Appendix B.

B. Slow quench with detuning ramp

Again motivated by Ref. [18], the second scenario we study is the dynamics as the longitudinal field Δ is slowly swept from far off resonance to the final detuning. For sufficiently slow ramps, coherent evolution, and no motional coupling, this would result in adiabatic preparation of the Ising ground state. The dynamics in Fig. 3 of Ref. [18] has three stages, where the first stage has large detuning. As the large detuning prevents atoms from being excited to the Rydberg state, the first stage has little to do with our estimate of the motional effect. Therefore, we omit this stage in our dynamics for simplicity and only model the next two stages (see Appendix C). Initially, all the atoms are prepared in the ground state under a laser field with Rabi frequency Ω_i and large laser detuning $\Delta_i \gg J$. The first stage of the ramping process is that the Δ decreases to a preset value Δ_f with a given ramp rate $\dot{\Delta}$ while Ω is constant. The second stage is a linear turnoff of the Ω with rate $\dot{\Omega}$ while Δ holds constant. We focus on the experimental parameter values $J = 2\pi \times 6$ MHz, $\Omega_i = 0.9J$, $\Delta_i = 3.3J$, and $\dot{\Omega} = 0.24J^2$. We incorporate the single-body decoherence into the calculations of the ramp dynamics, as described in Appendix A, to compare its effects with the motion-induced decoherence. We take the single-body decoherence times, specifically the lifetime and dephasing time, to be $T_1 = 20$ μs and $T_2 = 0.5$ μs, respectively.

Figure 3 shows results for two ramp rates $\dot{\Delta}$ in order to compare motional effects at different timescales. For the shortest duration ramps [Fig. 3(a) at positive Δ_f], the single-atom noise can play a more important role than the atom motion. However, the effect of motion rapidly appears and exceeds the single-atom noise, as seen in Fig. 3(a) for negative Δ_f and Fig. 3(b) for nearly all Δ_f. In Fig. 3(b), as the sweeping is slower (with smaller $\dot{\Delta}$), the process will be closer to an adiabatic process and build up a higher correlation peak. However, as this process takes a longer time, the effect of the atom motion is even larger.

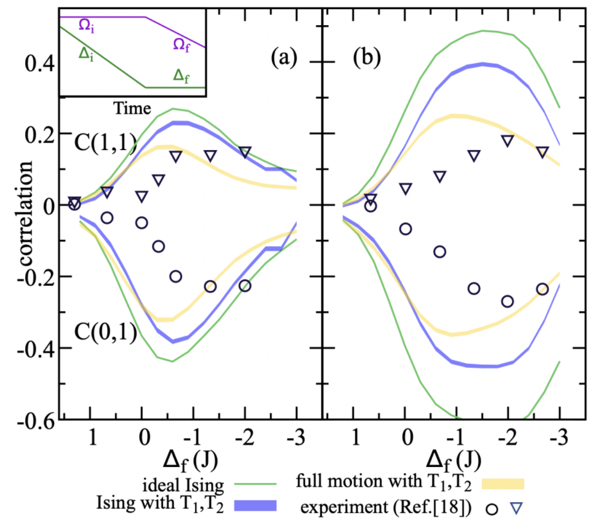

FIG. 3. Ramp results with varying Δ_f. (a) $\dot{\Delta} = -1.42J^2$. The fields Ω and Δ vary over time in two stages, as shown in the inset and described in the text. (b) $\dot{\Delta} = -0.70J^2$. The green curves are the ideal Ising results. The two shaded regions, which indicate ± 1 standard error of the mean, are the Ising and full-motion model results (blue and yellow curves, respectively), each with single-body T_1 and T_2 decoherence. Note that the horizontal axis is reversed. The circles and triangles are experimental data from Fig. 3 in Ref. [18].

The DTWA simulation supports the conjecture in Ref. [18] that atom motion is a significant source of decoherence in the detuning ramp results. Even though there are some differences between simulation and experiments that are possibly caused by either the limit of the DTWA method or the simplification in the model, the numerical results agree roughly with the experimentally observed correlations as a function of detuning [18] and give a peak magnitude quantitatively consistent with the experiment. The coherent results from the DTWA also agree with ED results (see Appendix C). As the atom motion is introduced to the model without any fitting, our results give a reasonable explanation the two-body interaction noise in Ref. [18].

IV. EFFECT OF MOTION IN OPTICAL TWEEZERS

The results above have shown the importance of motion in recent optical lattice experiments, raising the question of what role atom motion plays more generally in ongoing experiments with optical lattices and microtraps, another important technique to realize spin models with Rydberg atoms [11,13]. In this section we answer two relevant questions: First, what are possible ways to mitigate the motional effects in optical lattices? Second, what is the effect of atom motion in optical tweezer experiments?

A. Suppressing motional decoherence

Intuitively, the effect of motion will be smaller in a deeper lattice or with heavier atoms. Our calculations show that replacing lithium atoms with rubidium atoms or increasing the lattice depth can help reduce, but not eliminate, the motional effects, as shown in Fig. 4. In dynamics similar to the

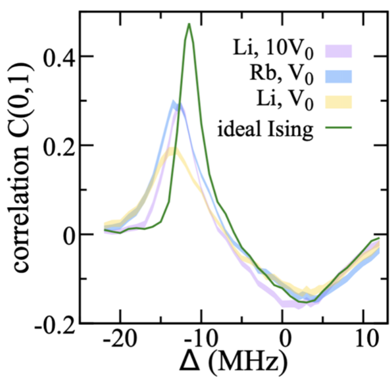

FIG. 4. Long-time ($\Omega t = 2.97\pi$) quench when Rb atoms are used or the depth of the lattice increases to $10V_0$, where V_0 is the lattice depth applied in Sec. III. These two results are plotted in comparison to the ideal Ising and full-motion results of the original setting. The shaded region indicates ±1 standard error of the mean.

long-time quench in Sec. III A 2 ($\Omega t = 2.97\pi$), using heavier atoms (Rb) or applying a deeper trap ($V = 10V_0$) increases the height of correlation peaks and is closer to the ideal Ising result. However, the peak remains much lower than in the ideal Ising dynamics and shifts noticeably. Because these techniques only partially alleviate the motional decoherence, atom motion will be important to consider when designing future experiments.

B. Motional decoherence in microtraps

Although the programmability of microtraps leads to a diversity of geometries, the effect of motion is generally expected to be smaller in microtraps than lattices, due to the microtraps' deeper wells. To evaluate these effects, we simulate the sudden quench dynamics with atom motion in microtraps in recently used experimental conditions with ^{87}Rb [11,45]. The parameters include $a_l = 10$ μm, $C_6/a_l^6 = \pm 2\pi \times 1.95$ MHz, $\Omega = 2\pi \times 1.95$ MHz, and a radial (longitudinal) harmonic-oscillator frequency near the trap center of 100 kHz (20 kHz).

The quench duration is 760 ns, which gives the same Ωt value as the long-time quench discussed in Sec. III A. The results are shown in Fig. 5, along with the DTWA results of the ideal Ising model for comparison. It should be noted that the atoms in microtraps are not fully cooled down after the preparation of the experiment. Thus, the initial conditions [Eq. (3)] correspond to the atoms' temperature in the magneto-optical trap, which is 25 μK [45].

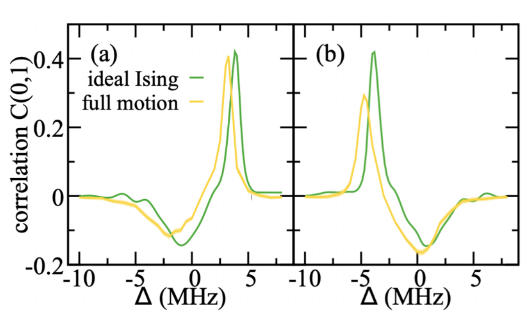

FIG. 5. Sudden quench results for a Rydberg-atom lattice based on Rb atoms trapped in microtraps, for different detuning values. The quench time is 760 ns ($\Omega t = 2.97\pi$). (a) $C(0, 1)$ with repulsive vdW interaction and (b) $C(0, 1)$ with attractive interaction. The shaded region indicates ±1 standard error of the mean.

Figure 5(a) shows that in microtraps with repulsive vdW interactions, a common case in experiments [11,13], the motional effects are fairly small in the timescale we consider. After the sudden quench, the full-motion model's peak in $C(0, 1)$ has the same height as in the ideal Ising model, but with a slightly shifted position.

An important point is that in ongoing microtrap experiments, Jt is 10 times larger than we consider here [11]. We have performed DTWA calculations for such timescales, seeing a much larger motional effect. This is not included in the figures because the strong quantum fluctuations and correlations at the longer times make our DTWA method questionable. Nevertheless, our results here suggest that the effect of motional decoherence should already be detectable at much shorter times and, as discussed in Sec. III A 2, it is reasonable to expect an increase in this motional effect at longer times.

Finally, we note that the sign of the interaction changes the motional effects as shown in Fig. 5(b). The effect of motion for repulsive interactions is less significant than that for attractive interactions. The $C(0, 1)$ in the attractive Rydberg-atom lattice [Fig. 5(b)] shows a suppression of peak height by the atom motion, which is not observed in the repulsive model in Fig. 5(a). The atom motion in the attractive model also shifts the peak position.

V. CONCLUSION

In summary, we showed that atom motion affects the evolution of correlations in Rydberg-atom lattices, which explains the discrepancy between coherent results and recent experimental observations. For example, the results indicate that atom motion suppresses magnetic correlations, sometimes by a large amount.

We also suggested possible ways to relieve the effect of atom motion including using heavier atoms, deeper lattices, or repulsive Rydberg-Rydberg interactions. All of these methods, which are usable in current experiments, can reduce, but not eliminate, the motional decoherence on the timescales we have considered. As the Rydberg-atom platforms become a major toolbox in quantum simulation and quantum computation, knowing the existence of motional decoherence, especially its magnitude in different timescales, is helpful to both design experiments and analyze results. Another route worth investigating to suppress motional decoherence is to use ultrafast dynamics, as in recent experiments in Refs. [3,46,47]. Here the short timescales minimize the thermal motion. If interaction-induced motion also remains slow compared to the ultrafast timescales, this platform may offer a route to simulate long-time spin dynamics with minimal motional effects.

Interesting future questions include how the motional dynamics interplays with other sources of noise including disorder in the lattice [11], blackbody-induced broadening [48,49] or transitions [50], motion-facilitated excitation [25,49], or interactions involving more than two bodies. The antitrapping force on Rydberg-state atoms in principle can have an important effect. In the regime of the current calculations, its effect is negligible compared to the interaction-induced motion. However, when the timescale is longer or the antitrapping potential much larger, it may induce atom motion or loss [51]. We have noticed that some quantitative differences remain between the DTWA simulation and experiments. To understand this, one may look to improve the motional Rydberg-atom lattice model to include the effects of longer-range interactions [18] and shapes of Rydberg-Rydberg interactions [20] and to extend the numerical methods to capture the strong quantum fluctuations that occur at timescales [36,52] that go beyond the current limit of DTWA methods.

ACKNOWLEDGMENTS

We thank F. Gao for conversations about related calculations. We acknowledge support from the Welch Foundation Grant No. C1872, W. M. Keck Foundation Grant No. 995764, the Office of Naval Research Grant No. N00014-20-1-2695, the National Science Foundation Grant No. PHY1848304, and Department of Energy Grant No. DE-SC0024301. K.R.A.H.'s contribution benefited from discussions at the KITP, which was supported in part by the National Science Foundation under Grant No. NSF PHY-1748958.

APPENDIX A: CLASSICAL EQUATION OF MOTION

According to the full master equation with the Hamiltonian (1) and the Lindblad jump terms, the classical equations of motion are

$$\dot{r}_i^\alpha = \frac{p_i^\alpha}{m}, \tag{A1}$$

$$\dot{p}_i^\alpha = -\sum_{j\in \mathrm{NN}\, i} \frac{3\hbar J a_l^6}{2r_{ij}^8}\left(r_i^\alpha - r_j^\alpha\right)\left(\sigma_i^z+1\right)\left(\sigma_j^z+1\right) - \frac{\hbar V_0 \pi^2}{a_l^2}\tilde{r}_i^\alpha\left(1-\sigma_i^z\right), \tag{A2}$$

$$\dot{\sigma_i^\alpha} = \left(\frac{\Delta}{2} + \sum_{j\in \mathrm{NN}\, i}\frac{J a_l^6}{2r_{ij}^6}\left(\sigma_j^z+1\right) + \frac{V_0\pi^2}{2a_l^2}\tilde{r}_i^2\right)\sum_\beta \epsilon^{\alpha\beta z}\sigma_i^\beta - \frac{\Omega}{2}\sum_\beta \epsilon^{\alpha\beta x}\sigma_i^\beta - \frac{1}{T_1}\left(-1+\sigma_i^z\right)\delta^{\alpha z} - \frac{1}{T_2}\sigma_i^\alpha\left(1-\delta^{\alpha z}\right), \tag{A3}$$

where ϵ^{ijk} is the Levi-Cività symbol, $\delta^{\alpha\beta}$ is the Kronecker delta, and the variables r_i^α, p_i^α, and σ_j^z are c-numbers corresponding to their quantum operator counterparts. In the calculation of the ramping dynamics in Sec. III B, we include the single-particle decay time T_1 and the dephasing time T_2 following the methods of Ref. [53] and compare the effects of single-body decoherence with those of the atom motion. To directly compare the motional dynamics to the Ising dynamics, both models exclude factors that may change T_1 and T_2, such as Doppler shift, ac Stark shift, magnetic-field inhomogeneity, and interplay between motion and single-particle decoherence. We expect these factors to be less impactful than atom motion. We also want to point out that an alternative way to incorporate the dissipative terms in TWA methods was recently developed in Ref. [54].

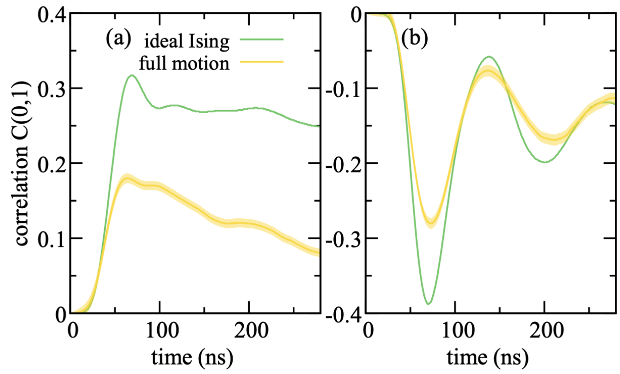

FIG. 6. Nearest-neighbor correlation $C(0,1)$ changes over time (a) off-resonance ($\Delta = -10$ MHz) and (b) at the single-atom resonance ($\Delta = 0$ MHz).

APPENDIX B: DEPENDENCE OF CORRELATIONS, KINETIC ENERGY, AND ATOM NUMBER ON TIME

To see how the effect of motion evolves, in Fig. 6 we show the values of the nearest-neighbor correlation $C(0,1)$ over time in the long-time quench at $\Delta = -10$ MHz (far from the single-particle resonance) and $\Delta = 0$ MHz (on resonance). These roughly are the detunings where atom motion has the largest and smallest effects, respectively. Figure 6 shows that the effect of motion accumulates over time, as the ideal Ising and full-motion curves overlap at the beginning of the quench, but start to show differences after $t = 50$ ns.

To gain insight into the role that atom motion plays in the dynamics, we examine the motional behavior directly. The average kinetic energy in Fig. 7 suggests that, when allowed to move, the kinetic energy of atoms will increase, especially in the in-plane direction. This is consistent with the effects of motional decoherence increasing over time during the quench.

Also, at long enough time some Rydberg atoms will get close enough to each other and react, leading to atom losses. To capture these numerically, we employ two approximate

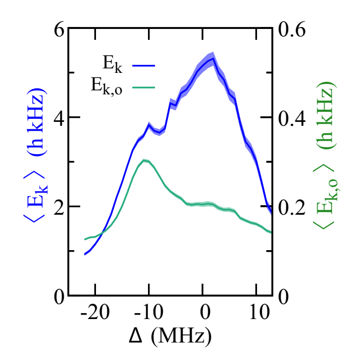

FIG. 7. Average kinetic energy (blue curve) and out-of-plane kinetic energy (green curve) at the end of the long-time quench as a function Δ. Initially, the zero-point energy per direction is $\hbar\omega/2 = h \times 0.108$ kHz.

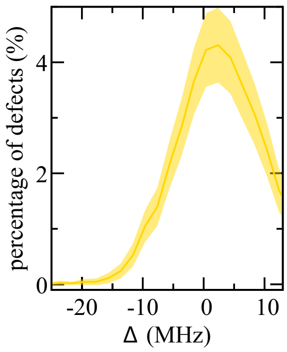

FIG. 8. Percentage of atom loss at the end of the long-time quench as a function of Δ.

criteria, as simulating the fast-timescale dynamics when two Rydberg atoms approach each other is challenging. First, when an atom moves out of its initial lattice site to a neighboring one, we take the pair of atoms to be lost. This is qualitatively accurate, as atoms typically only move so far when they are in the Rydberg state (due to their strong interactions with other Rydberg atoms), and when Rydberg atoms are close enough to be on the same site, their strong attractive interactions generally cause them to be lost. Second, we monitor the spin magnitude, and when due to the error caused by our finite time step it exceeds 0.9 (a coherent spin in the DTWA has a magnitude of $\frac{\sqrt{3}}{2} \approx 0.87$), we remove the atom from the system. This is a proxy for detecting when two Rydberg atoms approach so closely that the interactions are strong, and the atoms will quickly be attracted to each other and lost on a timescale on the order of our finite time step. (For our numerical time step, this threshold indicates that the atoms will approach within about less than $0.4a_0$ and therefore the two Rydberg-state atoms will likely react.) Two other extreme treatments are used to estimate the effect on correlation of this cutoff: One is freezing the Rydberg-state atom pair when they are about to collide; the other is normalizing the spin magnitude at each time step and keeping the dynamics. Both treatments give similar correlation within the size of the error bar even at resonance, which justifies the loss criteria. At the end of the dynamics, all lost atoms are treated as Rydberg-state atoms, according to the experimental detection techniques in Ref. [18]. However, as plotted in Fig. 8, after the long-time quench in Sec. III A 2, the fraction of motion-induced atom loss by the end of the dynamic is less than 5%, a small impact on the simulation results shown.

APPENDIX C: RAMP DYNAMICS

The accuracy of the DTWA for slow ramps in the absence of motion is checked with exact results, as shown in Fig. 9(a). These two sets of curves give similar shapes and the same position of the peak. We also simplify the three-stage quench dynamics to two stages, as the large detuning in the first stage prevents the excitation to the Rydberg state and has little to do with the motional effect. We further simplify the soft turnoff of the Rabi frequency to a linear ramp, which also does not qualitatively affect the results. Neither simplification

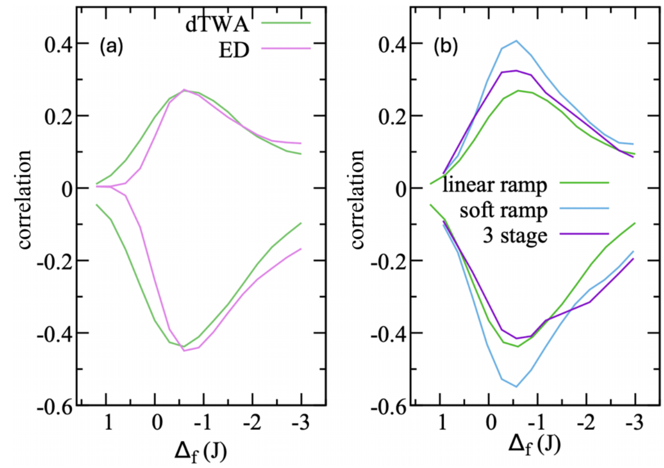

FIG. 9. (a) Comparison of ED results and coherent results from the DTWA for a slow ramp with $\dot{\Delta} = -1.42J^2$. (b) Comparison of the coherent short-time ramp dynamics of the full and simplified ramp protocols. The linear ramp has two-stage dynamics as presented in the main text. The soft ramp has two-stage dynamics with a soft turnoff of the Rabi frequency at the end. The curve labeled 3 stage shows the full experimental three-stage dynamics with a turn-on of Rabi frequency.

qualitatively affects the spin dynamics in the quench process, as shown in Fig. 9(b).

APPENDIX D: TRAPPING POTENTIAL

The trapping potential has a negligible effect on the dynamics, as illustrated in Fig. 10. In the example of a short-time quench, turning off the trapping-antitrapping potential results in minimal change to the nearest-neighbor correlation. In the comparison, we consider the antitrapping potential [55] $-\hbar V_R \frac{\pi^2}{2a_i^2}\tilde{r}_i^2(1+\sigma_i^z)$ and assume $V_R = V_0$. The convergence

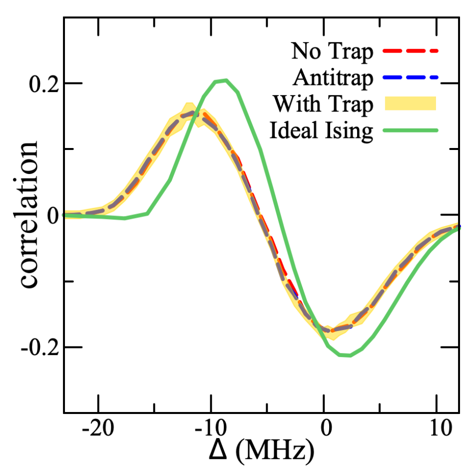

FIG. 10. Comparison of the nearest-neighbor correlation for different approximations to the short-time quench: thick yellow line, model with the ground-state trap; red dashed line, model without trapping potentials; and blue dashed line, model with the ground-state trap and Rydberg-state antitrap at the same magnitude. For reference, the curve for Ising-only dynamics (green solid) is also shown. Labels and curves are the same as in Fig. 2.

of three curves is also checked for ramp dynamics. The results show that the antitrapping force on Rydberg-state atoms, which is ignored in the main text, has little impact on the dynamics in this work.

[1] J. Zeiher, R. Van Bijnen, P. Schauß, S. Hild, J.-y. Choi, T. Pohl, I. Bloch, and C. Gross, Many-body interferometry of a Rydberg-dressed spin lattice, Nat. Phys. **12**, 1095 (2016).

[2] E. Guardado-Sanchez, B. M. Spar, P. Schauss, R. Belyansky, J. T. Young, P. Bienias, A. V. Gorshkov, T. Iadecola, and W. S. Bakr, Quench dynamics of a Fermi gas with strong nonlocal interactions, Phys. Rev. X **11**, 021036 (2021).

[3] V. Bharti, S. Sugawa, M. Mizoguchi, M. Kunimi, Y. Zhang, S. de Léséleuc, T. Tomita, T. Franz, M. Weidemüller, and K. Ohmori, Picosecond-scale ultrafast many-body dynamics in an ultracold Rydberg-excited atomic Mott insulator, Phys. Rev. Lett. **131**, 123201 (2023).

[4] H. Labuhn, D. Barredo, S. Ravets, S. de Léséleuc, T. Macrì, T. Lahaye, and A. Browaeys, Tunable two-dimensional arrays of single Rydberg atoms for realizing quantum Ising models, Nature (London) **534**, 667 (2016).

[5] D. Ohl de Mello, D. Schäffner, J. Werkmann, T. Preuschoff, L. Kohfahl, M. Schlosser, and G. Birkl, Defect-free assembly of 2D clusters of more than 100 single-atom quantum systems, Phys. Rev. Lett. **122**, 203601 (2019).

[6] F. M. Gambetta, W. Li, F. Schmidt-Kaler, and I. Lesanovsky, Engineering nonbinary Rydberg interactions via phonons in an optical lattice, Phys. Rev. Lett. **124**, 043402 (2020).

[7] H. Bernien, S. Schwartz, A. Keesling, H. Levine, A. Omran, H. Pichler, S. Choi, A. S. Zibrov, M. Endres, M. Greiner *et al.*, Probing many-body dynamics on a 51-atom quantum simulator, Nature (London) **551**, 579 (2017).

[8] H. Kim, Y. Park, K. Kim, H.-S. Sim, and J. Ahn, Detailed balance of thermalization dynamics in Rydberg-atom quantum simulators, Phys. Rev. Lett. **120**, 180502 (2018).

[9] V. Lienhard, S. de Léséleuc, D. Barredo, T. Lahaye, A. Browaeys, M. Schuler, L.-P. Henry, and A. M. Läuchli, Observing the space-and time-dependent growth of correlations in dynamically tuned synthetic Ising models with antiferromagnetic interactions, Phys. Rev. X **8**, 021070 (2018).

[10] S. de Léséleuc, S. Weber, V. Lienhard, D. Barredo, H. P. Büchler, T. Lahaye, and A. Browaeys, Accurate mapping of multilevel Rydberg atoms on interacting spin-1/2 particles for the quantum simulation of Ising models, Phys. Rev. Lett. **120**, 113602 (2018).

[11] P. Scholl, M. Schuler, H. J. Williams, A. A. Eberharter, D. Barredo, K.-N. Schymik, V. Lienhard, L.-P. Henry, T. C. Lang, T. Lahaye *et al.*, Quantum simulation of 2D antiferromagnets with hundreds of Rydberg atoms, Nature (London) **595**, 233 (2021).

[12] A. Browaeys and T. Lahaye, Many-body physics with individually controlled Rydberg atoms, Nat. Phys. **16**, 132 (2020).

[13] S. Ebadi, T. T. Wang, H. Levine, A. Keesling, G. Semeghini, A. Omran, D. Bluvstein, R. Samajdar, H. Pichler, W. W. Ho *et al.*, Quantum phases of matter on a 256-atom programmable quantum simulator, Nature (London) **595**, 227 (2021).

[14] G. Semeghini, H. Levine, A. Keesling, S. Ebadi, T. T. Wang, D. Bluvstein, R. Verresen, H. Pichler, M. Kalinowski, R. Samajdar, A. Omran, S. Sachdev, A. Vishwanath, M. Greiner, V. Vuletić, and M. D. Lukin, Probing topological spin liquids on a programmable quantum simulator, Science **374**, 1242 (2021).

[15] Y. Song, M. Kim, H. Hwang, W. Lee, and J. Ahn, Quantum simulation of Cayley-tree Ising Hamiltonians with three-dimensional Rydberg atoms, Phys. Rev. Res. **3**, 013286 (2021).

[16] A. Dauphin, M. Müller, and M. A. Martin-Delgado, Quantum simulation of a topological Mott insulator with Rydberg atoms in a Lieb lattice, Phys. Rev. A **93**, 043611 (2016).

[17] F. Grusdt, M. Kánasz-Nagy, A. Bohrdt, C. S. Chiu, G. Ji, M. Greiner, D. Greif, and E. Demler, Parton theory of magnetic polarons: Mesonic resonances and signatures in dynamics, Phys. Rev. X **8**, 011046 (2018).

[18] E. Guardado-Sanchez, P. T. Brown, D. Mitra, T. Devakul, D. A. Huse, P. Schauß, and W. S. Bakr, Probing the quench dynamics of antiferromagnetic correlations in a 2D quantum Ising spin system, Phys. Rev. X **8**, 021069 (2018).

[19] W. Li, C. Ates, and I. Lesanovsky, Nonadiabatic motional effects and dissipative blockade for Rydberg atoms excited from optical lattices or microtraps, Phys. Rev. Lett. **110**, 213005 (2013).

[20] T. Macri and T. Pohl, Rydberg dressing of atoms in optical lattices, Phys. Rev. A **89**, 011402(R) (2014).

[21] M. Genkin, S. Wüster, S. Möbius, A. Eisfeld, and J. Rost, Dipole-dipole induced global motion of Rydberg-dressed atom clouds, J. Phys. B **47**, 095003 (2014).

[22] T. Keating, R. L. Cook, A. M. Hankin, Y.-Y. Jau, G. W. Biedermann, and I. H. Deutsch, Robust quantum logic in neutral atoms via adiabatic Rydberg dressing, Phys. Rev. A **91**, 012337 (2015).

[23] L. F. Buchmann, K. Mølmer, and D. Petrosyan, Creation and transfer of nonclassical states of motion using Rydberg dressing of atoms in a lattice, Phys. Rev. A **95**, 013403 (2017).

[24] A. Mitra, M. J. Martin, G. W. Biedermann, A. M. Marino, P. M. Poggi, and I. H. Deutsch, Robust Mølmer-Sørensen gate for neutral atoms using rapid adiabatic Rydberg dressing, Phys. Rev. A **101**, 030301(R) (2020).

[25] L. Festa, N. Lorenz, L.-M. Steinert, Z. Chen, P. Osterholz, R. Eberhard, and C. Gross, Blackbody-radiation-induced facilitated excitation of Rydberg atoms in optical tweezers, Phys. Rev. A **105**, 013109 (2022).

[26] F. Robicheaux, T. M. Graham, and M. Saffman, Photon-recoil and laser-focusing limits to Rydberg gate fidelity, Phys. Rev. A **103**, 022424 (2021).

[27] M. Magoni, P. Mazza, and I. Lesanovsky, Phonon dressing of a facilitated one-dimensional Rydberg lattice gas, SciPost Phys. Core **5**, 041 (2022).

[28] Y. Dudin and A. Kuzmich, Strongly interacting Rydberg excitations of a cold atomic gas, Science **336**, 887 (2012).

[29] S. Baur, D. Tiarks, G. Rempe, and S. Dürr, Single-photon switch based on Rydberg blockade, Phys. Rev. Lett. **112**, 073901 (2014).

[30] M. M. Müller, M. Murphy, S. Montangero, T. Calarco, P. Grangier, and A. Browaeys, Implementation of an experimentally feasible controlled-phase gate on two blockaded Rydberg atoms, Phys. Rev. A **89**, 032334 (2014).

[31] J. Han, T. Vogt, and W. Li, Spectral shift and dephasing of electromagnetically induced transparency in an interacting Rydberg gas, Phys. Rev. A **94**, 043806 (2016).

[32] M. Marcuzzi, J. Minář, D. Barredo, S. de Léséleuc, H. Labuhn, T. Lahaye, A. Browaeys, E. Levi, and I. Lesanovsky, Facilitation dynamics and localization phenomena in Rydberg lattice gases with position disorder, Phys. Rev. Lett. **118**, 063606 (2017).

[33] J. Schachenmayer, A. Pikovski, and A. M. Rey, Many-body quantum spin dynamics with Monte Carlo trajectories on a discrete phase space, Phys. Rev. X **5**, 011022 (2015).

[34] R. Khasseh, A. Russomanno, M. Schmitt, M. Heyl, and R. Fazio, Discrete truncated Wigner approach to dynamical phase transitions in Ising models after a quantum quench, Phys. Rev. B **102**, 014303 (2020).

[35] M. Kunimi, K. Nagao, S. Goto, and I. Danshita, Performance evaluation of the discrete truncated Wigner approximation for quench dynamics of quantum spin systems with long-range interactions, Phys. Rev. Res. **3**, 013060 (2021).

[36] S. Czischek, M. Gärttner, M. Oberthaler, M. Kastner, and T. Gasenzer, Quenches near criticality of the quantum Ising chain—power and limitations of the discrete truncated Wigner approximation, Quantum Sci. Technol. **4**, 014006 (2018).

[37] A. Polkovnikov, Phase space representation of quantum dynamics, Ann. Phys. (NY) **325**, 1790 (2010).

[38] L. Pucci, A. Roy, and M. Kastner, Simulation of quantum spin dynamics by phase space sampling of Bogoliubov-Born-Green-Kirkwood-Yvon trajectories, Phys. Rev. B **93**, 174302 (2016).

[39] O. L. Acevedo, A. Safavi-Naini, J. Schachenmayer, M. L. Wall, R. Nandkishore, and A. M. Rey, Exploring many-body localization and thermalization using semiclassical methods, Phys. Rev. A **96**, 033604 (2017).

[40] B. Sundar, K. C. Wang, and K. R. A. Hazzard, Analysis of continuous and discrete Wigner approximations for spin dynamics, Phys. Rev. A **99**, 043627 (2019).

[41] J. Schachenmayer, A. Pikovski, and A. M. Rey, Dynamics of correlations in two-dimensional quantum spin models with long-range interactions: A phase-space Monte-Carlo study, New J. Phys. **17**, 065009 (2015).

[42] A. Signoles, T. Franz, R. Ferracini Alves, M. Gärttner, S. Whitlock, G. Zürn, and M. Weidemüller, Glassy dynamics in a disordered Heisenberg quantum spin system, Phys. Rev. X **11**, 011011 (2021).

[43] A. Schuckert, I. Lovas, and M. Knap, Nonlocal emergent hydrodynamics in a long-range quantum spin system, Phys. Rev. B **101**, 020416(R) (2020).

[44] W. K. Wootters, A Wigner-function formulation of finite-state quantum mechanics, Ann. Phys. (NY) **176**, 1 (1987).

[45] D. Barredo, V. Lienhard, S. de Leseleuc, T. Lahaye, and A. Browaeys, Synthetic three-dimensional atomic structures assembled atom by atom, Nature (London) **561**, 79 (2018).

[46] N. Takei, C. Sommer, C. Genes, G. Pupillo, H. Goto, K. Koyasu, H. Chiba, M. Weidemüller, and K. Ohmori, Direct observation of ultrafast many-body electron dynamics in an ultracold Rydberg gas, Nat. Commun. **7**, 13449 (2016).

[47] C. Sommer, G. Pupillo, N. Takei, S. Takeda, A. Tanaka, K. Ohmori, and C. Genes, Time-domain Ramsey interferometry with interacting Rydberg atoms, Phys. Rev. A **94**, 053607 (2016).

[48] E. A. Goldschmidt, T. Boulier, R. C. Brown, S. B. Koller, J. T. Young, A. V. Gorshkov, S. L. Rolston, and J. V. Porto, Anomalous broadening in driven dissipative Rydberg systems, Phys. Rev. Lett. **116**, 113001 (2016).

[49] T. Boulier, E. Magnan, C. Bracamontes, J. Maslek, E. A. Goldschmidt, J. T. Young, A. V. Gorshkov, S. L. Rolston, and J. V. Porto, Spontaneous avalanche dephasing in large Rydberg ensembles, Phys. Rev. A **96**, 053409 (2017).

[50] J. A. Aman, B. J. DeSalvo, F. B. Dunning, T. C. Killian, S. Yoshida, and J. Burgdörfer, Trap losses induced by near-resonant Rydberg dressing of cold atomic gases, Phys. Rev. A **93**, 043425 (2016).

[51] R. J. P. T. de Keijzer, O. Tse, and S. J. J. M. F. Kokkelmans, Recapture probability for antitrapped Rydberg states in optical tweezers, Phys. Rev. A **108**, 023122 (2023).

[52] J. Wurtz, A. Polkovnikov, and D. Sels, Cluster truncated Wigner approximation in strongly interacting systems, Ann. Phys. (NY) **395**, 341 (2018).

[53] V. P. Singh and H. Weimer, Driven-dissipative criticality within the discrete truncated Wigner approximation, Phys. Rev. Lett. **128**, 200602 (2022).

[54] C. D. Mink, D. Petrosyan, and M. Fleischhauer, Hybrid discrete-continuous truncated Wigner approximation for driven, dissipative spin systems, Phys. Rev. Res. **4**, 043136 (2022).

[55] S. K. Dutta, J. R. Guest, D. Feldbaum, A. Walz-Flannigan, and G. Raithel, Ponderomotive optical lattice for Rydberg atoms, Phys. Rev. Lett. **85**, 5551 (2000).